

Vertical vibrations of composite bridge/track structure/high-speed train systems. Part 3: Deterministic and random vibrations of exemplary system

M. PODWORNA¹ and M. KLASZTORMY^{2*}

¹ Institute of Civil Engineering, Wroclaw University of Technology, 27 Wyspianskiego St., 50-370 Wroclaw, Poland

² Department of Mechanics and Applied Computer Science, Military University of Technology, 2 Kaliskiego St., 00-908 Warsaw, Poland

Abstract. Based on the one-dimensional quasi-exact physical and mathematical modelling of a composite (steel-concrete) bridge/track structure/high-speed train system (BTT), developed in Part 2, advanced computer algorithms for the BTT numerical modelling and simulation as well as a computer programme to simulate vertical vibrations of BTT systems are developed. The exemplary bridge under numerical quasi-static and dynamic analysis, designed according to Polish standards, has a 15.00 m span length and belongs to the SCB series-of-types developed in Part 1. The bridge is loaded by a German ICE-3 high-speed train moving at the resonant and maximum operating speeds. A continuously welded ballasted track structure adapted to high operating velocities is applied. The output quantities include: time-histories of the vertical deflection of the main beams at the midspan, time-histories of the longitudinal normal stress in the bottom fibres of the main beams at the midspan, time-histories of the vertical acceleration of the bridge deck at the midspan, time-histories of the vertical accelerations of the suspension pivots in car-bodies, time-histories of the dynamic pressures of the wheel sets of moving rail-vehicles. The design quantities, understood as the extreme values of the output quantities, are used to verify the design conditions. The basic random factor, i.e. vertical track irregularities of the track, is taken into consideration. Basic statistics of the design quantities treated as random variables are calculated and taken into account in the design conditions.

Key words: composite steel-concrete bridge, ballasted track structure, high-speed train, design, simulation, random vertical track irregularities, numerical analysis.

1. Introduction

The problems developed in the contribution are based on Refs. [1-14]. The authors have designed a series-of-types of symmetrical composite (steel – concrete) railway bridges, as well as transition zones and a track structure, all adapted to passenger trains operating at high speeds of up to 300 km/h [8]. The bridge examined numerically in this study has a 15.00 m span length and the assigned code SCB-15. In [9], the authors developed a theory of one-dimensional (1D) quasi-exact physical and mathematical modelling of composite (steel-concrete) bridge/track structure/high-speed train system (BTT) systems, including viscoelastic suspensions of rail-vehicles having two two-axle bogies each, non-linear Hertz contact stiffness and one-sided contact between the wheel sets and the rails, viscoelastic and inertia features of the bridge, the track structure on and beyond the bridge, the approach slabs, and random vertical track irregularities. Based on this theory, the authors developed advanced computer algorithms for the BTT numerical modelling and simulation and a computer programme to simulate vertical vibrations of BTT systems. The quasi-static and dynamic analysis was conducted with respect to the SCB-15 bridge loaded by a German ICE-3 high-speed train.

In reference to modelling of random track irregularity samples, only the vertical profile (elevation irregularity), i.e. the mean vertical elevation of two rails, is taken into consid-

eration [9]. Short wavelength corrugation irregularities in rail and design geometry irregularities in track formation are neglected. A stationary and ergodic Gaussian process in space, describing vertical irregularities, is characterised by a one-sided power spectral density (PSD) function $S_{rr}(\Omega)$, with $\Omega = 2\pi/L_r$ [rad/m] as the spatial frequency, and L_r as wavelength. The most common definition of $S_{rr}(\Omega)$ is presented in [12, 13] and was elaborated by Federal Railroad Administration (FRA USA) in the form

$$S_{rr}(\Omega) = kA \frac{\Omega_c^2}{(\Omega^2 + \Omega_c^2) \Omega^2} \left[\frac{\text{mm}^2 \text{m}}{\text{rad}} \right], \quad (1)$$

where $k = 0.25$, $\Omega_c = 0.8245$ [rad/m] and coefficient A [$\text{mm}^2 \text{rad/m}$] is specified for line grades 1 – 6. Only the better railway lines of grades, i.e. 4 ($A = 53.76$), 5 ($A = 20.95$), and 6 ($A = 3.39$), are considered in this study.

Random samples of the track irregularity vertical profile are generated with the Monte-Carlo method which results in the following formula [12, 13]

$$r(x) = 2 \sum_{i=1}^{N_r} \sqrt{S_{rr}(\Omega_i) \Delta \Omega} \cos(\Omega_i x + \phi_i) \quad [\text{mm}], \quad (2)$$

where $\Omega_i = \Omega_{\min} + (i - 0.5)\Delta\Omega$ – discrete frequency, ϕ_i – random phase angle uniformly distributed over $[0, 2\pi]$ [rad] interval and independent for $i = 1, 2, \dots, N_r$,

*e-mail: m.klasztorny@gmail.com

$\Delta\Omega = \frac{1}{N_r} (\Omega_{\max} - \Omega_{\min})$ – frequency increment, N_r – total number of frequency increments in $[\Omega_{\min}, \Omega_{\max}]$ interval, $\Omega_{\min} = \frac{2\pi}{L_{r,\max}} \Omega_{\max} = \frac{2\pi}{L_{r,\min}}$ – lower and upper limits of spatial frequency, $L_{r,\min}, L_{r,\max}$ – lower and upper limits of wavelength.

Taking into account the experimental data available in [1–3, 5, 6, 11–14], the values $L_{r,\min} = 0.10$ m, $L_{r,\max} = 70.00$ m are assumed as adequate to simulate vibrations of single span bridges of span length to 30.00 m. Based on the preliminary simulations, value of $N_r = 100$ was assessed to be the most adequate to obtain the correct output samples close to reality. Figure 1 presents a random sample of vertical track irregularities for $N_r = 100$.

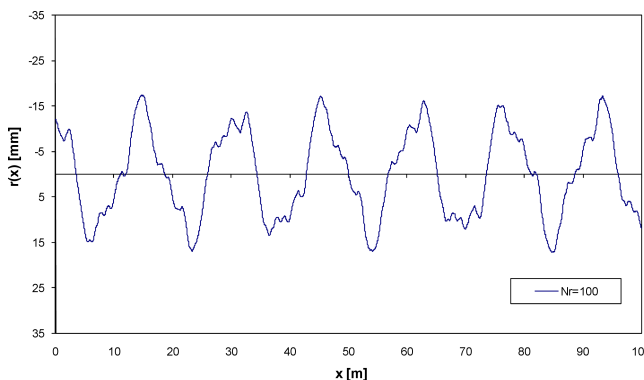


Fig. 1. Sample of vertical track irregularities for line grade 4

The contribution presents the results of quasi-static and dynamic analysis of the exemplary BTT system, i.e. the SCB-15 bridge/ballasted track structure/ICE-3 train system. The results are illustrated graphically and numerically. The dynamic processes are simulated for the resonant operating speeds $v_{31} = 180$ km/h and $v_{21} = 270$ km/h and for the maximum operating speed $v_{\max} = 300$ km/h.

2. Shortened description of BTT system and sets of input data

The BTT system is composed of a simply supported composite bridge, two approach slabs, a track structure with continuously welded rails and a high-speed train. The 1D physical and mathematical modelling of the BTT system is based on the following assumptions and ideas [9]. There is considered a finitely long deformable continuously welded track including the out-of-transition zones, the transition zones and the bridge zone. The track outside of these zones is non-deformable and straight. There may occur random vertical track irregularities identical for both main rails, described by a spatial function $r(x)$ which is a stationary ergodic Gaussian process defined by the PSD function determined experimentally. The BTT system has a vertical plane of symmetry coinciding with the track axis; this is the plane of vibration. The operating and side rails are viscoelastic prismatic beams deformable in flexure. The sleepers vibrate vertically and are modelled as point masses. The ballast is modelled as a set of

vertical viscoelastic constraints with non-linear elastic characteristics. The ballast mass is discretized. Potential separation of the sleepers from the ballast is taken into consideration. The track-bed (subsoil) is a linearly viscoelastic layer with lumped mass distribution. The approach slabs are modelled as viscoelastic prismatic beams deformable in flexure. The bridge superstructure is reflected by a simply-supported, stepwise-prismatic beam, deformable in flexure, symmetrical relative to the bridge midspan. A set of eight rail-vehicles form a high-speed ICE-3 German train. Each vehicle has two independent two-axle bogies. The planar Matsuura model of a rail-vehicle is adopted in the extended version via inclusion of non-linear one-sided contact Hertz springs at wheel sets – rail contacts. Potential micro-separations of the moving wheels from the rails and potential impacts are taken into account. Vibrations of the BTT system are physically nonlinear and geometrically linear.

A finitely long section of the deformable track is depicted in Fig. 2. The following symbols defined in [9] are introduced: v – operating velocity of train, $w(x, t)$ – vertical deflection of bridge superstructure, $\sigma(x, t)$ – longitudinal normal stresses in bottom fibres of main beams, t – time variable, x, y – coordinates, $a_p(x, t)$ – vertical acceleration of bridge platform, $R_{ki}(t)$, $k = 1, 2, 3, 4$, $i = 1, 2, \dots, N_v$ – dynamic pressures of moving wheel sets, $k = 1, 2, 3, 4$ – numbering of wheel sets of i^{th} vehicle, N_v – number of vehicles forming train, $a_{bi\alpha}(t)$, $i = 1, 2, \dots, N_v$, $\alpha = f, r$ – vertical accelerations of suspension pivots in car-bodies (f, r – front/rear bogie), T – dynamic process duration time, $L_o = L + 2L_a$ – bridge span length L plus lengths of approach slabs plus two sleeper intervals, L_v – train set length.

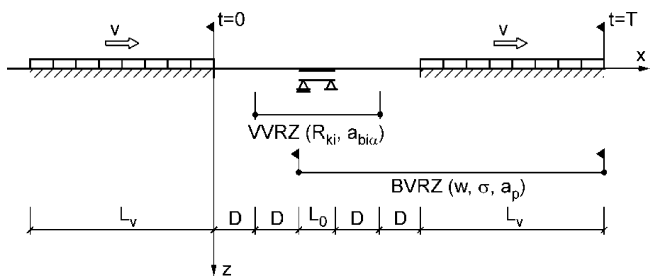


Fig. 2. Schematic diagram of BTT system at time $t = 0$ and $t = T$, Ref [9]

The out-of-approach zones have $2D$ length. The first D section, measured from the train entering side, enters subsequent vehicles into the quasi-stationary random vibration state. The Vehicle Vibration Registration Zone (VVRZ) is the area of registration of the design quantities found in the traffic safety condition (TSC) and the passenger comfort conditions (PCC) conditions defined in further considerations. The Bridge Vibration Registration Zone (BVRZ) is the area of registration of the vibrations and stresses in relation to the bridge superstructure and the platform. The wheel set/rails interaction forces are recorded during the passage of the selected axle over the VVRZ zone, including micro-separations of the wheels from the rails.

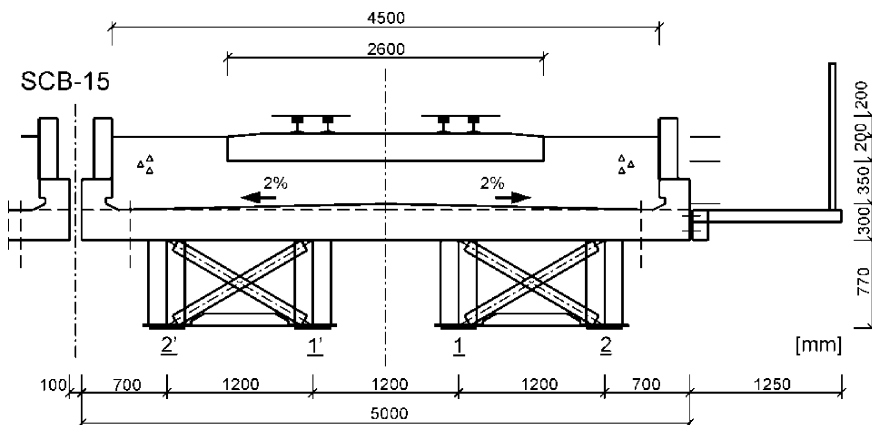


Fig. 3. Fully symmetric cross-section of SCB-15 bridge at midspan, Ref [8]

The fully symmetric cross-section of the exemplary SCB-15 bridge at the midspan, with glass-fibre reinforced plastic (GFRP) shell walls used to protect the ballast-bed, is depicted in Fig. 3 [8]. New structural features of the bridge as collected below:

- a fully symmetric reinforced concrete (RC) platform (minimization of the flexural – torsional vibrations, elimination of through-the-ballast vibration coupling of adjacent parallel bridge spans),
- low concrete kerbs, structurally reinforced and multiply dilated, on both sides of the platform plate (elimination of one-side RC platform wall inducing asymmetric vibrations of the bridge superstructure and increasing lateral and flexural – torsional vibrations),
- multiply dilated GFRP laminate shells used to hold ballast in the platform bed,
- four I-shape main beams joined in two pairs with horizontal and vertical wind bracing,
- rolling bearings, unmovable laterally under two internal main beams (better horizontal load capacity),
- thicker back wall of the abutment to support the approach slabs with elastomeric bearings.

Physical and geometric parameters of the SCB-15 bridge are set up in Table 1.

A ballasted track structure is designed to suit the operating speeds to 300 km/h [8]. The track structure components are: 60E1 (UIC-60) operating and side rails, Vossloh 300-1 fasteners of operating and side rails, B 320 U60/B 320 U60-

U sleepers, a ballast layer of 35 cm thick under the sleepers in the track axis, reinforced concrete (RC) approach slabs, cement-stabilized subsoil in the approach zones, a sand-gravel mix upper layer, an unwoven fabric – reinforced embankment in the out-of-approach zones. The elastic characteristics of Vossloh 300-1 fastening pair is non-linear. Macadam ballast is a linearly elastic layer at compression and does not transmit tension. The fastenings and the ballast exhibit damping properties approximated as linear viscous damping. Physical and geometric parameters of the track structure are summarized in Table 2.

ICE-3 high-speed trains were built by Siemens Company in 2000 and 2001 in the total number of 50 trains (Series 1). The ICE-3 (Inter City Express) is the third generation of German high-speed trains. The main difference in comparison to the previous generations is a multiple unit power system, i.e. the train has motor bogies located every second car. The total weight is distributed evenly across the entire trainset, therefore the axle loads for all cars are equal to 16 metric tons. The maximum operating velocity of ICE-3 trains equals 300 km/h. The ICE-3 train set contains 8 rail-vehicles. Configuration of the four end cars is a mirror reflection of the four front cars which are set as follows: PC – a power car supported on two SF 500 TDG motor bogies, TC – a transformer car supported on two SF 500 TDG trailer bogies, CC – a converter car supported on two SF 500 TDG motor bogies, IC – an intermediate car supported on two SF 500 TDG trailer bogies [10].

Table 1
Physical and geometric parameters of SCB-15 bridge, Ref [8]

Parameter	Symbol	Unit	Value
bridge span length	L	m	15.00
distance of bottom fibres of main beams from neutral axis	$h_b(0.5L)$	mm	735
bending ratio for bottom fibres of bridge superstructure cross section, at midspan	$W_b(0.5L)$	m^3	0.092242
flexural rigidity for $\bar{x} \in [0.2L; 0.8L]$, $\bar{x} = x - (2D + L_a + d)$	$EI(0.5L)$	Nm^2	13.897×10^9
flexural rigidity for $\bar{x} \in [0; 0.2L](0.8L; L]$	$EI(0)$	Nm^2	10.289×10^9
mass per unit length for $\bar{x} \in [0.2L; 0.8L]$	$m(0.5L)$	kg/m	5300
mass per unit length for $\bar{x} \in [0; 0.2L](0.8L; L]$	$m(0)$	kg/m	5050
quasi-constant damping ratio in frequency range $[f_l, f_u]$ (Rayleigh damping model)	γ	–	0.01125

Table 2
Physical and geometric parameters of track structure, Ref [10]

Parameter	Unit	Value
<i>60E1 rails pair (both operating and side)</i>		
flexural stiffness, $E_r I_r$	MN·m ²	12.22
mass per unit length, m_r	kg/m	120
damping ratio, γ_r	–	0.004
<i>Vossloh 300-I fasteners pair</i>		
dynamic stiffness in compression in range of $0 - u_f$, k_{f1} ($u_f = 1$ mm)	MN/m	51
dynamic stiffness in compression in range of $> u_f$, k_{f2} ($u_f = 1$ mm)	MN/m	90
dynamic stiffness in tension, k_{f3}	MN/m	9
viscous damping coefficient, c_f	kN·s/m	75
<i>B 320 U60 / B 320 U60-U sleeper</i>		
spacing, d	m	0.60
mass of sleeper and fasteners pair, M_s	kg	366
<i>ballast-bed</i>		
ballast mass per one sleeper, M_b	kg	2900
dynamic stiffness in compression, k_{b1}	MN/m	180
dynamic stiffness in tension, k_{b2}	MN/m	0
viscous damping coefficient, c_b	kN·s/m	60
<i>approach slab</i>		
span length, L_a	m	4.70
mass per unit length, m_a	kg/m	2000
Young's modulus, E_a	MPa	34 600
flexural stiffness, $E_a I_a$	MN·m ²	92.3
damping ratio, γ_a	–	0.015
<i>track bed</i>		
dynamic stiffness, k_g	MN/m	150
viscous damping coefficient, c_g	kN·s/m	30

The enhanced Matsuura model of a rail-vehicle is depicted in Fig. 4 [9]. Wheel sets of the vehicle are modelled as point masses vibrating vertically, each with 1DOF. Bogie frames are modelled as rigid disks, each with 2DOF (vertical translation

and rotation). The car body is also modelled as a rigid disk with 2DOF. The suspensions of the first and second stage are linear viscoelastic. The first-stage suspension pivots are at the same height as the mass centre of the bogie. The second-stage

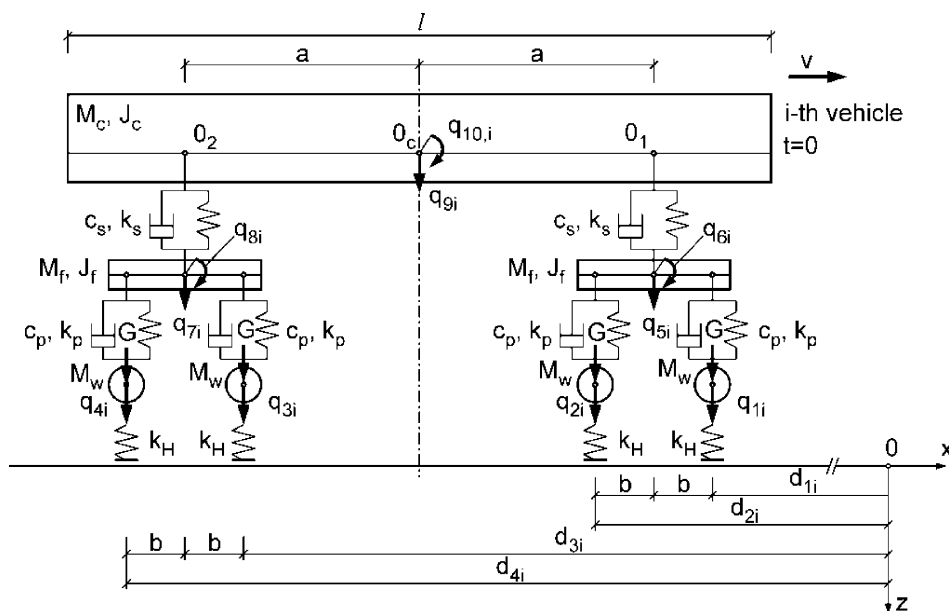


Fig. 4. Enhanced Matsuura model of rail-vehicle and its position at $t = 0$, Ref [9]

Vertical vibrations of composite bridge/track structure/high-speed train systems. Part 3

suspension pivots are at the same height as the mass centre of the car body. The masses modelling the wheel sets are fitted with one-sided vertical springs of nonlinear Hertzian contact stiffness k_H reflecting wheel set – rails contact. The interaction force per wheel set, carried by the vertical spring of stiffness k_H , equals [5, 9]

$$R = 2(k_H u_H)^{3/2}, \quad (3)$$

where u_H – shortening of vertical spring, $k_H = 0.216 \times 10^8 \left[\frac{\text{N}^{2/3}}{\text{m}} \right]$ – average value of contact stiffness.

The parameters corresponding to planar models of the power, transformer, converter and intermediate cars in the ICE-3 train are provided in Tables 3 and 4, respectively. Part of the ICE-3 parameters, not available in the literature, were estimated using respective parameters of the Shinkansen high-speed train [7].

Table 3

Parameters for power and converter cars of ICE-3 train, Ref [10]

Parameter	Unit	Value
mass of car body, M_c	kg	45 600
mass of bogie frame, M_f	kg	4400
mass of wheel set, M_w	kg	2400
central moment of inertia for body, J_c	$\text{kg} \cdot \text{m}^2$	2 397 000
central moment of inertia for bogie frame, J_f	$\text{kg} \cdot \text{m}^2$	5420
total equivalent vertical stiffness per axle, k_p	kN/m	1124
total equivalent vertical damping per axle, c_p	kN·s/m	8.8
total equivalent vertical stiffness per bogie, k_s	kN/m	561
total equivalent vertical damping per bogie, c_s	kN·s/m	27
total car length, l	m	24.78
bogie base, $2a$	m	17.38
axle base (in bogie), $2b$	m	2.50
nominal radius of new wheel tread	m	0.460
axle load per gravity acceleration $g = 9.81 \text{ m/s}^2$, G/g	kg	16 000

Table 4
Parameters for transformer and intermediate cars of ICE-3 train, Ref [10]

Parameter	Unit	Value
mass of car body, M_c	kg	49 000
mass of bogie frame, M_f	kg	2700
mass of wheel set, M_w	kg	2400
central moment of inertia for body, J_c	$\text{kg} \cdot \text{m}^2$	2 576 000
central moment of inertia for bogie frame, J_f	$\text{kg} \cdot \text{m}^2$	3330
total equivalent vertical stiffness per axle, k_p	kN/m	690
total equivalent vertical damping per axle, c_p	kN·s/m	5.4
total equivalent vertical stiffness per bogie, k_s	kN/m	603
total equivalent vertical damping per bogie, c_s	kN·s/m	29
total car length, l	m	24.78
bogie base, $2a$	m	17.38
axle base (in bogie), $2b$	m	2.50
nominal radius of new wheel tread	m	0.460
axle load per gravity acceleration $g = 9.81 \text{ m/s}^2$, G/g	kg	16 000

The BTT system is divided into the following natural subsystems: BS – bridge superstructure, LAS – left approach slab, RAS – right approach slab, LB – left ballast-bed, RB – right ballast-bed, SL – sleepers, OR – operating rails, SR – side rails, $RV_i, i = 1, 2, \dots, N_v$ – set of moving rail-vehicles (N_v – number of rail-vehicles). The 1D physical model of the track structure/bridge subsystem is presented in Fig. 5 [9]. Beams modelling operating rails, side rails, approach slabs and the bridge superstructure are discretised using beam finite elements deformable in flexure, with 4DOF and length d (sleepers spacing). Finite element nodes correspond to the positions of sleepers at intervals d . The ballast-bed mass on the approach slabs and on the bridge was taken as uniformly distributed. Step-wise changes in the parameters of the bridge superstructure are in the relevant finite element nodes. The physical model of the track/bridge subsystem is symmetrical relative to the midspan of the bridge, with the exception of random track irregularities.

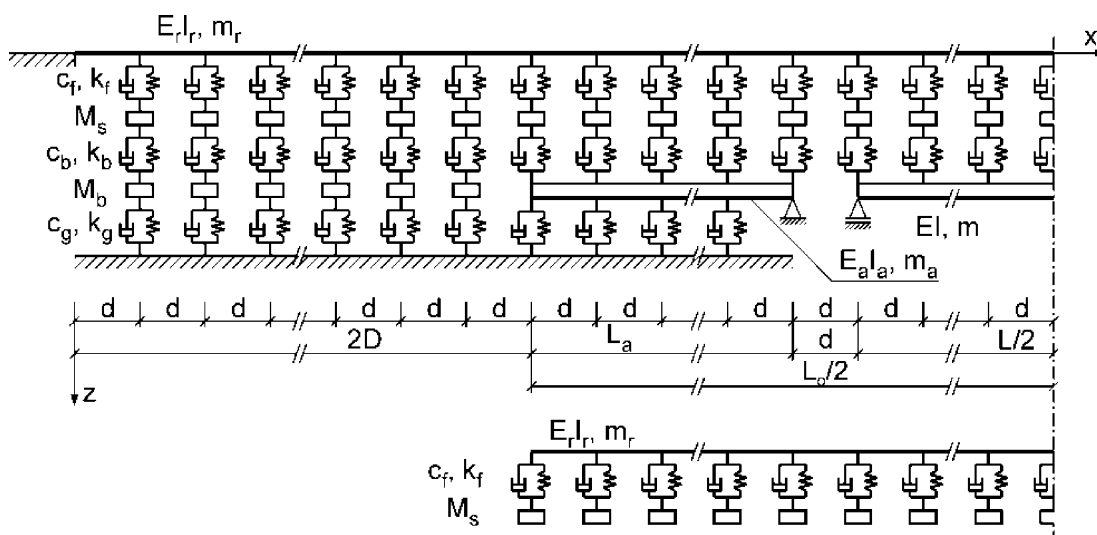


Fig. 5. 1D physical model of track structure/bridge subsystem, Ref [9]

The subsystems constituting the BTT system are subject to relevant subsets of the vertical interaction forces carried by the elastic/viscoelastic, physically linear/nonlinear constraints, specified and illustrated in [9]. Making the use of the Lagrange equations (of the first and second order) and internal assembling of the subsystems meshed according to FEM, one obtains matrix equations of motion of the BTT subsystems, with explicit linear left sides and implicit nonlinear right-side vectors expressed in terms of the interaction forces. Coupling of these equations and non-linearity is hidden in the general load vectors. Such formulation leads to matrix equations of motion with constant coefficients and the recurrent – iterative numerical integration algorithm as presented in [9].

The transient and quasi-steady-state vibrations of the BTT system are governed by $8 + N_v$ matrix equations of motion in the following implicit form [9]:

$$\begin{aligned} \mathbf{B}\ddot{\mathbf{q}} + \mathbf{C}\dot{\mathbf{q}} + \mathbf{K}\mathbf{q} &= \mathbf{F}, \\ \mathbf{B}_{la}\ddot{\mathbf{q}}_{la} + \mathbf{C}_{la}\dot{\mathbf{q}}_{la} + \mathbf{K}_{la}\mathbf{q}_{la} &= \mathbf{F}_{la}, \\ \mathbf{B}_{ra}\ddot{\mathbf{q}}_{ra} + \mathbf{C}_{ra}\dot{\mathbf{q}}_{ra} + \mathbf{K}_{ra}\mathbf{q}_{ra} &= \mathbf{F}_{ra}, \\ \{\mathbf{M}_b\}\ddot{\mathbf{q}}_{lb} &= \mathbf{F}_{lb}, \\ \{\mathbf{M}_b\}\ddot{\mathbf{q}}_{rb} &= \mathbf{F}_{rb}, \\ \{\mathbf{M}_s\}\ddot{\mathbf{q}}_s &= \mathbf{R}_f - \mathbf{R}_b, \\ \mathbf{B}_r\ddot{\mathbf{q}}_r + \mathbf{C}_r\dot{\mathbf{q}}_r + \mathbf{K}_r\mathbf{q}_r &= \mathbf{F}_r, \\ \mathbf{B}_{sr}\ddot{\mathbf{q}}_{sr} + \mathbf{C}_{sr}\dot{\mathbf{q}}_{sr} + \mathbf{K}_{sr}\mathbf{q}_{sr} &= \mathbf{F}_{sr}, \\ \mathbf{B}_i\ddot{\mathbf{q}}_i &= \mathbf{F}_i, \quad i = 1, 2, \dots, N_v, \end{aligned} \quad (4)$$

where $\mathbf{q}(t)$, $\mathbf{q}_{la}(t)$, $\mathbf{q}_{ra}(t)$, $\mathbf{q}_{lb}(t)$, $\mathbf{q}_{rb}(t)$, $\mathbf{q}_s(t)$, $\mathbf{q}_r(t)$, $\mathbf{q}_{sr}(t)$ – vectors of generalised coordinates for BS, LAS, RAS, LB, RB, SL, OR, SR subsystems, respectively, $\mathbf{q}_i(t)$, $i = 1, 2, \dots, N_v$ – vectors of generalised coordinates for subsequent rail-vehicles, \mathbf{B} , \mathbf{C} , \mathbf{K} – mass, damping and stiffness matrices for BS subsystem, respectively, \mathbf{B}_{la} , \mathbf{C}_{la} , \mathbf{K}_{la} , \mathbf{B}_{ra} , \mathbf{C}_{ra} , \mathbf{K}_{ra} – mass, damping and stiffness matrices for LAS and RAS subsystems, respectively, $\{\mathbf{M}_b\}$ – mass matrix for LB and RB subsystems, $\{\mathbf{M}_s\}$ – mass matrix for SL subsystem, \mathbf{B}_r , \mathbf{C}_r , \mathbf{K}_r , \mathbf{B}_{sr} , \mathbf{C}_{sr} , \mathbf{K}_{sr} – mass, damping and stiffness matrices for OR and SR subsystems, respectively, \mathbf{B}_i – mass matrix for i^{th} rail-vehicle, \mathbf{R}_f , \mathbf{R}_{sf} – vectors of interaction forces transmitted by fasteners in OR and SR subsystems, respectively, \mathbf{R}_b – vector of interaction forces transmitted by ballast-bed, \mathbf{R}_g – vector of interaction forces transmitted by track-bed, \mathbf{R}_{wi} – vector of moving pressure forces of i^{th} vehicle wheel sets acting on rails, $\mathbf{F}(\mathbf{R}_b)$ – generalised load vector in implicit form, related to BS subsystem, $\mathbf{F}_{la}(\mathbf{R}_b, \mathbf{R}_g)$, $\mathbf{F}_{ra}(\mathbf{R}_b, \mathbf{R}_g)$ – generalised load vectors in implicit form, related to LAS and RAS subsystems, respectively, $\mathbf{F}_{lb}(\mathbf{R}_b, \mathbf{R}_g)$, $\mathbf{F}_{rb}(\mathbf{R}_b, \mathbf{R}_g)$ – generalised load vectors in implicit form, related to LB and RB subsystems, respectively, $\mathbf{F}_r(\mathbf{R}_f, \mathbf{R}_{wi})$, $i = 1, 2, \dots, N_v$, $\mathbf{F}_{sr}(\mathbf{R}_{sf})$ – generalised load vectors in implicit form, related to OR and SR subsystems, respectively, $\mathbf{R}_i = \text{col}(R_{1i} \ R_{2i} \ \dots \ R_{10,i})$ – vec-

tor of vertical interactions transmitted by 1st and 2nd stage suspensions of i^{th} vehicle, \mathbf{G} – generalised load vector reflecting static pressures of wheel sets onto rails, $\mathbf{F}_i(\mathbf{R}_i, \mathbf{G})$, $i = 1, 2, \dots, N_v$ – generalised load vector in implicit form, related to RVi , $i = 1, 2, \dots, N_v$ subsystem, $\cdot = d/dt$ – differentiation with respect to time variable t . Detailed formulae defining matrices and vectors in Eqs. (4) are given in [9].

In the case of an ICE 3 train, the wheel – rail static pressures for all axles and are equal to $G = 16000 \text{ kg} \times 9.81 \frac{\text{m}}{\text{s}^2} = 156.96 \text{ kN}$. The static shortening of contact springs is (see Eq. (3)) $u_{Ho} = (0.5G)^{2/3}/k_H = (0.5 \times 156960)^{2/3}/(0.216 \times 10^8) = 84.86 \times 10^{-6} \text{ m}$.

3. Additional problems

3.1. Prediction of forced resonances. A new concept of prediction of the forced resonances in BTT systems is developed in [8]. The results are collected below. Preliminary calculations identifying the fundamental natural quasi-frequency of the physically nonlinear bridge/track structure subsystem are made for a selected operating speed, taking into consideration quasi-free damped vibrations induced by the passage of the train. Approximate values of the fundamental natural quasi-period and the fundamental natural quasi-frequency of the bridge/track subsystem are calculated from the formulae

$$T_1 = \frac{s}{v}, \quad f_1 = \frac{1}{T_1}, \quad (5)$$

where s – distance of the load front during one cycle of quasi-free damped vibrations. Periods of subsequent harmonics of the quasi-static excitation of the bridge/track subsystem are

$$\bar{T}_i = \frac{l}{iv}, \quad i = 1, 2, \dots \quad (6)$$

Prediction of the resonant operation speeds, resulting from equality of the fundamental natural quasi-period and subsequent harmonics of the quasi-static excitation, $T_1 = \bar{T}_i$, is as follows

$$v = v_{i1} = \frac{l}{iT_1}, \quad i = 1, 2, \dots \quad (7)$$

where (see Tables 3 and 4) $l = 24.78 \text{ m}$.

Due to parametric effects resulting from quasi unsprung moving masses (wheel sets), the more exact resonant operating speeds are lower by $\sim 1.5\%$ compared to the values calculated from Eq. (7). Predicted resonant operating speeds decreased by $\sim 1.5\%$, in reference to the SCB-15 bridge, are collected in Table 5.

Table 5
Predicted resonant operation speeds in reference to the SCB-15 bridge

Bridge	T ₁	f ₁	v ₁₁	v ₂₁	v ₃₁	v ₄₁	v ₅₁
	[s]	[1/s]	[km/h]				
SCB-15	0.163	6.14	540	270	180	135	108

3.2. Parameters for numerical integration of equations of motion. The implicit matrix equations of motion (4), governing parametric – forced nonlinear vibrations of coupled subsystems of the BTT system, are integrated numerically

using the Newmark average acceleration method with parameters $\beta_N = 1/4$, $\gamma_N = 1/2$, developed to the implicit form in [9]. This method is not affected with an amplitude error. The initial value of a numerical integration time step can be assumed based on the accuracy condition put on the period error in reference to oscillations with the local frequency corresponding to wheel sets, according to the formulae:

- average contact stiffness in the static equilibrium of ICE-3 train

$$k_o = \frac{G}{u_o} = \frac{156960}{0.00008486} = 18.5 \times 10^8 \left[\frac{\text{N}}{\text{m}} \right], \quad (8)$$

- local natural frequency of ICE-3 train wheel set

$$f_o = \frac{1}{2\pi} \sqrt{\frac{k_o}{M_w}} = \frac{1}{2\pi} \sqrt{\frac{18.5 \times 10^8}{2400}} = 140 \text{ Hz}, \quad (9)$$

- time step equal to 0.01 of local period $T_o = 1/f_o$

$$h = \frac{T_o}{100} = \frac{1}{14000} = 7.14 \times 10^{-5} \text{ s}, \quad (10)$$

- initial value of time step: $h = 10^{-5}$ s.

The final value of a time step $h = 2 \times 10^{-5}$ s was assumed based on preliminary simulations of the BTT dynamic response.

The extreme values of the output quantities were searched in each time step while time histories were registered with a bigger output step corresponding to 2000 output points. The parameter ε in the iteration ending condition was assumed to be equal to $\varepsilon = 10^{-8}$ N. The allowed number of iterations equalled 15.

4. Output and design quantities

4.1. Dynamic response of bridge. Dynamic response of the bridge due to a high-speed passenger train moving at operating speed v can be characterised by time-histories of the vertical deflection of the main beams at the midspan and the longitudinal normal stress in the bottom fibres of the main beams at the midspan. The following output quantities are registered using the virtual model of the BTT system:

- dynamic vertical deflection $w(0.5L, t)$, simulated without or with random track irregularities, for selected resonant and extraresonant operating speeds,
- quasi-static vertical deflection $w_s(0.5L, t)$, simulated for $v = 30$ km/h (no random track irregularities taken into account),
- dynamic amplification factor for vertical deflection

$$\varphi_w(0.5L) = \frac{\max_t w(0.5L, t)}{\max_t w_s(0.5L, t)}, \quad (11)$$

- dynamic longitudinal normal stress $\sigma(0.5L, t)$, simulated without or with random track irregularities, for selected resonant and extra resonant operating speeds,

- quasi-static longitudinal normal stress $\sigma_s(0.5L, t)$, simulated for $v = 30$ km/h (no random track irregularities taken into account),
- dynamic amplification factor for longitudinal normal stress in bottom fibres of main beams at midspan

$$\varphi_\sigma(0.5L) = \frac{\max_t \sigma(0.5L, t)}{\max_t \sigma_s(0.5L, t)}. \quad (12)$$

The values of $w\sigma$ are recorded when the train head is in the range $[2D, 4D + L_o + L_v]$.

In order to assess fatigue durability of the bridge superstructure, the load capacity condition (LCC), related to longitudinal normal stress in the bottom fibres of the main beams at the midspan, is assumed in the form [4]

$$\begin{aligned} \sigma_f(0.5L) &= \sigma_{gk}(0.5L) + \sigma_m(0.5L) \\ &+ \zeta \sigma_a(0.5L) \leq \sigma_{\lim}. \end{aligned} \quad (13)$$

where $\sigma_f(0.5L)$ – equivalent normal stress including high-cycle fatigue, $\sigma_{gk}(0.5L) = 33.47$ MPa – normal stress due to characteristic weight of bridge [8], $\sigma_m(0.5L)$ – average normal stress corresponding to extreme quasi-steady-state vibrations, $\sigma_a(0.5L)$ – amplitude of normal stress corresponding to extreme quasi-steady-state vibrations, ζ – high-cycle fatigue factor, σ_{\lim} – admissible normal stress.

Relationship (13) is obtained from the Schmidt graph approximated with broken line, assuming a constant safety factor. If condition (13) is satisfied, full durability of the bridge with a safety margin is protected. For S235W structural steel, the high-cycle fatigue factor is $\zeta = 2.35$, and the admissible normal stress equals $\sigma_{\lim} = f_{yk}/n_s = 235/1.5 = 157$ MPa, where f_{yk} – yield strength, n_s – safety coefficient [4].

4.2. Traffic safety and passenger comfort conditions. The traffic safety condition (TSC) and the passenger comfort condition (PCC) are discussed in detail in [8]. The results are collected below. The PCC is expressed by the maximum vertical deflection of the bridge span which is equal to $w_{\lim} = L/1700$. The maximum permitted peak value of bridge deck acceleration calculated along the line of a track shall not exceed the design value $a_{p,\lim} = 3.50 \text{ m/s}^2$ for ballasted track. Verifications on bridge deformations, performed for PCC, can be related to vertical deflection of the deck or directly to the car body vertical acceleration. The indicative levels of comfort, expressed by the vertical acceleration $a_{b,\lim}$ inside the carriage during the travel are specified in Table 6 (EN 1990 Eurocode: *Basis of structural design. Annex A2: Application for bridges*).

Table 6
The indicative levels of passenger comfort (EN 1990 Eurocode)

Level of comfort	$a_{b,\lim} [\text{m/s}^2]$
very good	1.0
good	1.3
acceptable	2.0

Based on [9], UIC (Draft) Code 776-2 (2003), *Design requirements for rail bridges based on interaction phenomena between train, track, bridge and in particular speed*, Paris, France, Union Int. des Chemins de Fer, EN 1991-2, Eurocode 1: Actions on structures. Part 2: General actions – traffic loads on bridges, the traffic safety condition (TSC) for the BTT system is assumed in the form:

$$a_{p,\max} = \max_t |\ddot{w}(0.5L, t)| \leq a_{p,\lim}, \quad (14)$$

where $\ddot{w}(0.5L, t)$ – vertical acceleration of bridge superstructure at the midspan, simulated without or with random track irregularities, for selected resonant and extraresonant operating speeds, $a_{p,\max}$ – extreme vertical acceleration of the bridge deck at the midspan, during the passage of the train through the BVRZ zone, $a_{p,\lim} = 3.50 \text{ m/s}^2$ – admissible vertical acceleration of the bridge deck at the midspan.

Based on [9], UIC (Draft) Code 776-2 (2003), EN 1990 Eurocode, EN 1991-2 Eurocode 1, the passenger comfort condition (PCC) has the form:

$$a_{b,\max} = \max_t |a_{bi\alpha}(t)| \leq a_{b,\lim}, \quad (15)$$

$$i = 1, 2, \dots, N_v, \quad \alpha = f, r,$$

where $a_{bi\alpha}(t)$ – vertical accelerations of suspension pivots in subsequent car bodies, simulated without or with random track irregularities, for selected resonant and extraresonant operating speeds, $a_{b,\max}$ – extreme vertical acceleration of suspension pivots in subsequent car bodies, during passage of i^{th} vehicle through VVRZ zone, $a_{b,\lim}$ – admissible vertical acceleration inside carriage during travel, specified in Table 5, with (see Fig. 4)

$$a_{bif}(t) = \ddot{q}_{9i}(t) + a\ddot{q}_{10,i}(t), \quad (16)$$

$$a_{bir}(t) = \ddot{q}_{9i}(t) - a\ddot{q}_{10,i}(t).$$

In other words, values of a_p are recorded when the front of the train is in the range $[2D, 4D + L_o + L_v]$. On the other hand, the a_b values are recorded when the front of the i^{th} vehicle is in the range $[D, 4D + L_o]$.

4.3. Dynamic pressures of wheel sets onto rails. The values of dynamic pressures of the wheel sets onto the rails, i.e. $R_{ki}(t)$, $k = 1, 2, 3, 4$, $i = 1, 2, \dots, N_v$, are recorded during the passage of the front of the i^{th} vehicle through the interval $[D, 4D + L_o]$. At the initial time the dynamic pressures of wheel sets are G . The design quantity is defined as the minimum value of all dynamic pressures of wheel sets onto rails, i.e.

$$R_{\min} = \min_t R_{ki}(t), \quad (17)$$

$$k = 1, 2, 3, 4, \quad i = 1, 2, \dots, N_v.$$

4.4. Design quantities as random continuous variables. Vertical track irregularities are a random factor in the phys-

ically nonlinear BTT system. Random samples of these irregularities are calculated using the Monte-Carlo method, according to Eq. (2). Six design quantities were defined in previous considerations, i.e. $\varphi_w(0.5L)$, $\varphi_\sigma(0.5L)$, $\sigma_f(0.5L)$, $a_{p,\max}(0.5L)$, $a_{b,\max}$, R_{\min} , and they can be treated as random continuous variables.

Let Z is a selected random continuous variable. One considers an n – element simple random sample, where $n = N_{rs}$, i.e. (Z_1, Z_2, \dots, Z_n) . The value of the random sample is (z_1, z_2, \dots, z_n) . Basic statistics (expectance $E(Z)$, variance $D^2(Z)$, standard deviation $D(Z)$) of the n – element sample are defined by well-known formulae, i.e.

$$\bar{Z}_n = \frac{1}{n} \sum_{k=1}^n Z_k, \quad (18)$$

$$S_n^2 = \frac{1}{n} \sum_{k=1}^n (Z_k - \bar{Z}_n)^2,$$

$$S_n = \sqrt{S_n^2}.$$

The estimators of these statistics are respectively

$$\bar{z}_n = \frac{1}{n} \sum_{k=1}^n z_k, \quad (19)$$

$$s_n^2 = \frac{1}{n} \sum_{k=1}^n (z_k - \bar{z}_n)^2,$$

$$s_n = \sqrt{s_n^2}.$$

5. Numerical analysis of exemplary system

Based on the vibration theory developed in [9] and the numerical problems considered in previous points, the authors developed respective advanced computational algorithms and elaborated a computer programme in DELPHI to simulate deterministic or random vertical vibrations of BTT systems.

The simulations were conducted for an ICE-3 train moving at the most dangerous resonant operating velocities, i.e. $v_{31} = 180 \text{ km/h}$ (resonance of first quasi-modal system with third harmonic of static periodic moving load), $v_{21} = 270 \text{ km/h}$ (resonance of first quasi-modal system with second harmonic of static periodic moving load) and at the maximum operating velocity $v_{\max} = 300 \text{ km/h}$. The extreme values of the output quantities are given in Table 7, with $w_{\max} = \max_t w(0.5L, t)$, $\sigma_{\max} = \max_t \sigma(0.5L, t)$.

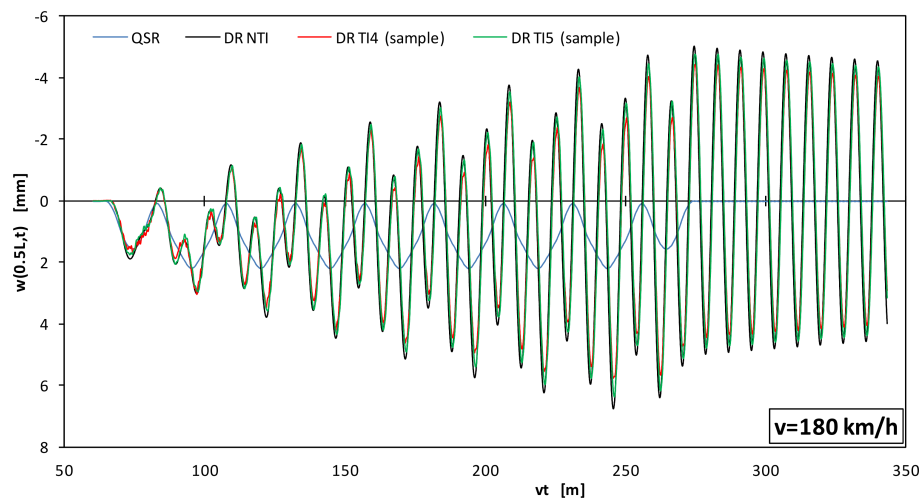
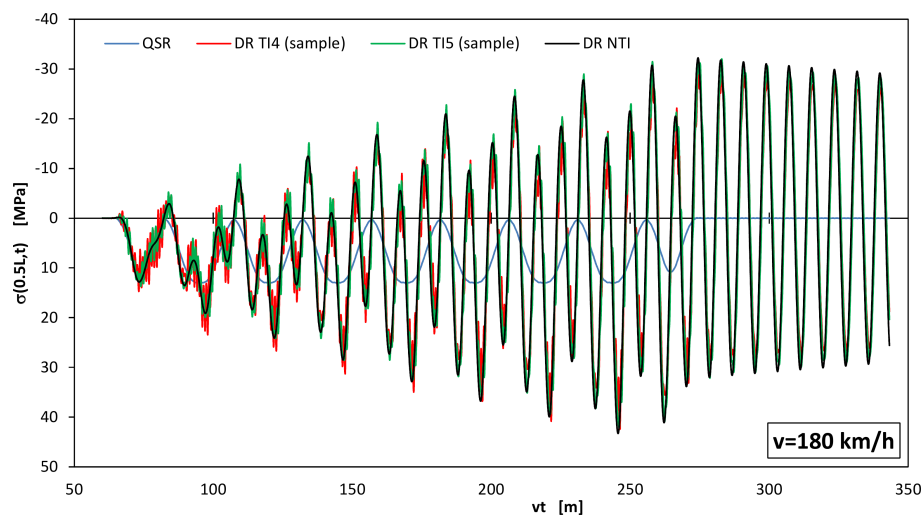
Figures 6–20 present time-histories of selected output quantities for resonant service velocities v_{31} , v_{21} and for the maximum velocity v_{\max} , respectively. The following codes are introduced in both Figs. 6–20 and in Table 7: QSR – quasi-static response, DR – dynamic response, (sample) – random simulation example, NTI – no track irregularities, TI4, TI5, TI6 – random track irregularities at line grades 4, 5, 6, respectively.

Vertical vibrations of composite bridge/track structure/high-speed train systems. Part 3

Table 7

Extreme values of output quantities in reference to SCB-15 bridge/ballasted track structure/ICE-3 high-speed train system

Task	w_{\max} [mm]	σ_{\max} [MPa]	$a_{p,\max}$ [m/s ²]	$a_{b,\max}$ [m/s ²]	R_{\min} [kN]
$v = 30 \text{ km/h, QSR, NTI}$	2.20	13.00	0.02	0.03	156.38
$v_{31} = 180 \text{ km/h, DR, NTI}$	6.74	43.29	7.44	0.24	141.43
$v_{31} = 180 \text{ km/h, DR, TI6 (sample)}$	6.92	44.78	9.56	0.42	49.87
$v_{31} = 180 \text{ km/h, DR, TI5 (sample)}$	6.39	42.06	12.92	0.66	0
$v_{31} = 180 \text{ km/h, DR, TI4 (sample)}$	5.76	42.42	16.29	1.08	0
$v_{21} = 270 \text{ km/h, DR, NTI}$	5.82	38.25	6.12	0.22	136.51
$v_{21} = 270 \text{ km/h, DR, TI6 (sample)}$	5.99	40.01	10.25	0.40	21.16
$v_{21} = 270 \text{ km/h, DR, TI5 (sample)}$	6.57	44.39	18.03	0.63	0
$v_{21} = 270 \text{ km/h, DR, TI4 (sample)}$	4.95	43.62	57.88	1.10	0
$v_{\max} = 300 \text{ km/h, DR, NTI}$	4.37	27.18	3.75	0.12	138.74
$v_{\max} = 300 \text{ km/h, DR, TI6 (sample)}$	4.28	27.51	6.47	0.23	0
$v_{\max} = 300 \text{ km/h, DR, TI5 (sample)}$	4.29	29.26	12.71	0.41	0
$v_{\max} = 300 \text{ km/h, DR, TI4 (sample)}$	4.19	33.84	34.85	0.74	0

Fig. 6. SCB-15 bridge/ballasted track structure/ICE-3 high-speed train system. Output quantity $w(0.5L, t)$ [mm] at resonant service velocity $v_{31} = 180 \text{ km/h}$ Fig. 7. SCB-15 bridge/ballasted track structure/ICE-3 high-speed train system. Output quantity $\sigma(0.5L, t)$ [MPa] at resonant service velocity $v_{31} = 180 \text{ km/h}$

M. Podworna and M. Klasztor

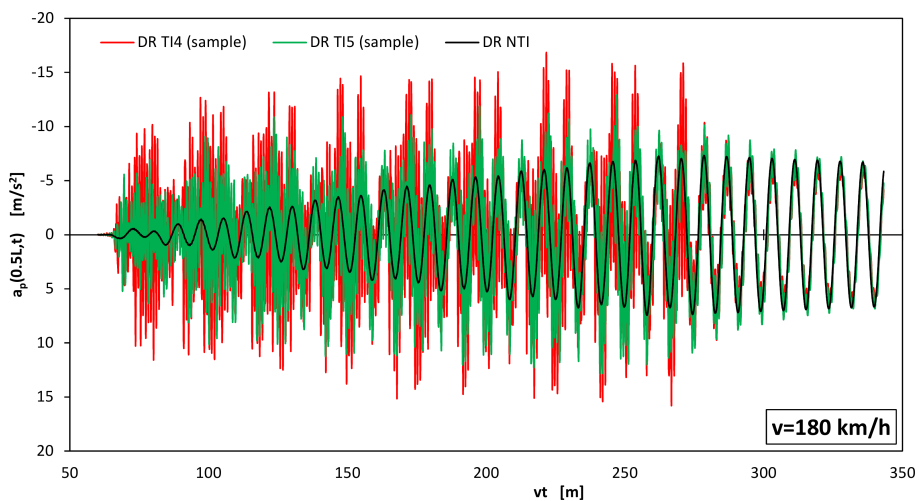


Fig. 8. SCB-15 bridge/ballasted track structure/ICE-3 high-speed train system. Output quantity $a_p(0.5L, t)$ [m/s^2] at resonant service velocity $v_{31} = 180 \text{ km/h}$

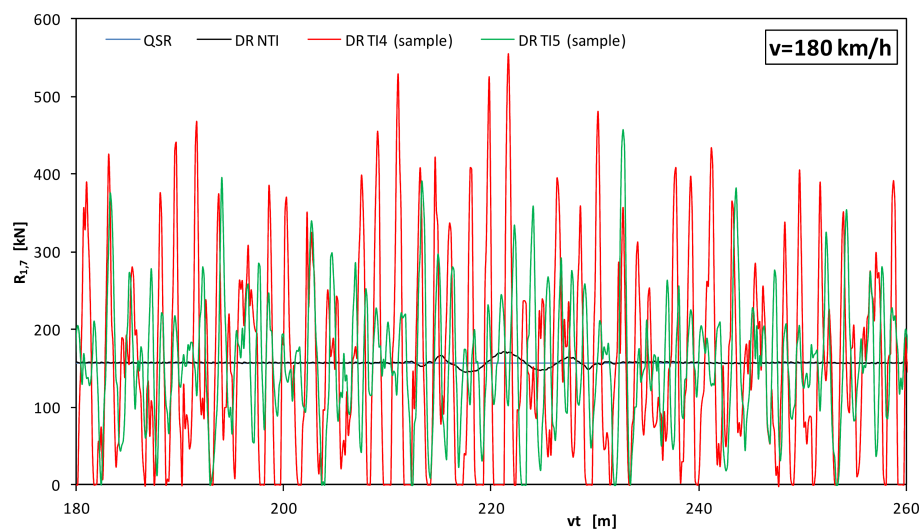


Fig. 9. SCB-15 bridge/ballasted track structure/ICE-3 high-speed train system. Output quantity $R_{1,7}(t)$ [kN] at resonant service velocity $v_{31} = 180 \text{ km/h}$

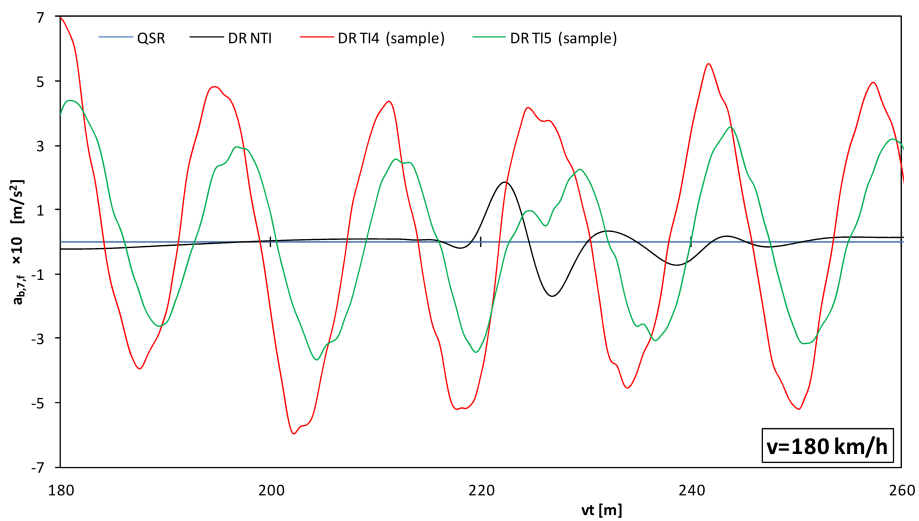


Fig. 10. SCB-15 bridge/ballasted track structure/ICE-3 high-speed train system. Output quantity $a_{b,7,f}(t)$ [m/s^2] at resonant service velocity $v_{31} = 180 \text{ km/h}$

Vertical vibrations of composite bridge/track structure/high-speed train systems. Part 3

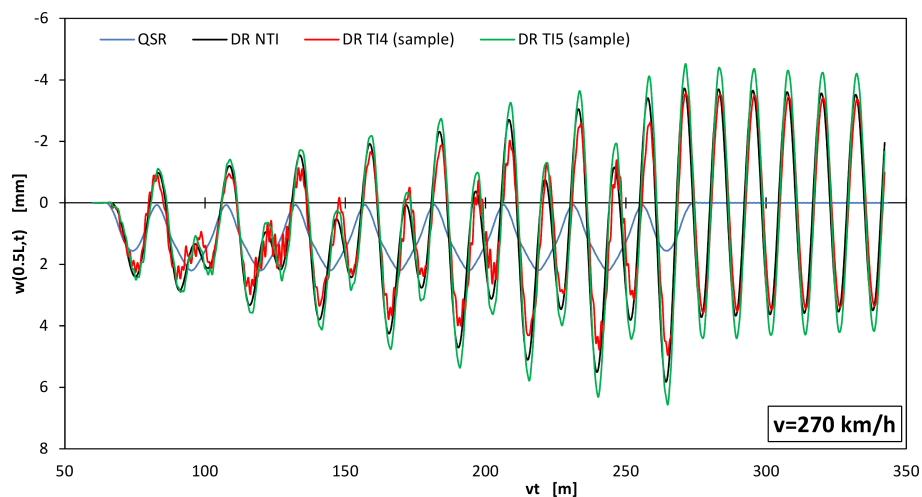


Fig. 11. SCB-15 bridge/ballasted track structure/ICE-3 high-speed train system. Output quantity $w(0.5L, t)$ [mm] at resonant service velocity $v_{21} = 270 \text{ km/h}$

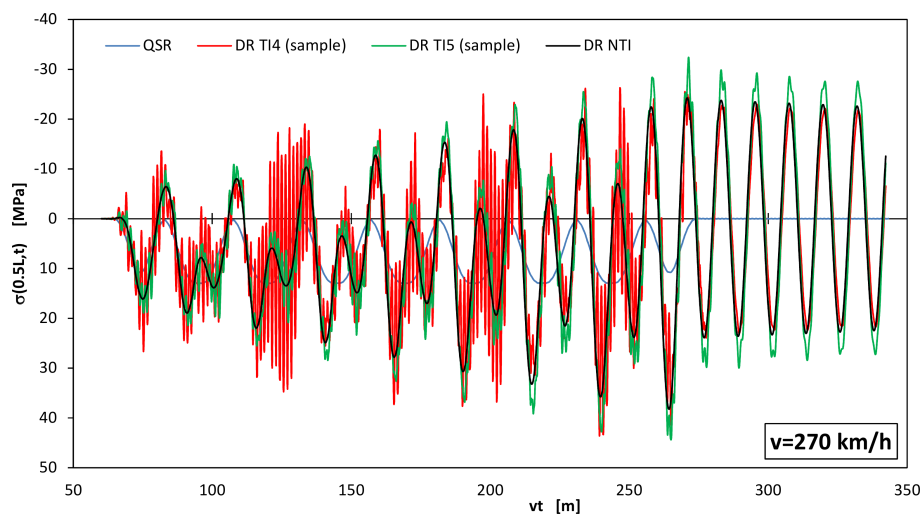


Fig. 12. SCB-15 bridge/ballasted track structure/ICE-3 high-speed train system. Output quantity $\sigma(0.5L, t)$ [MPa] at resonant service velocity $v_{21} = 270 \text{ km/h}$

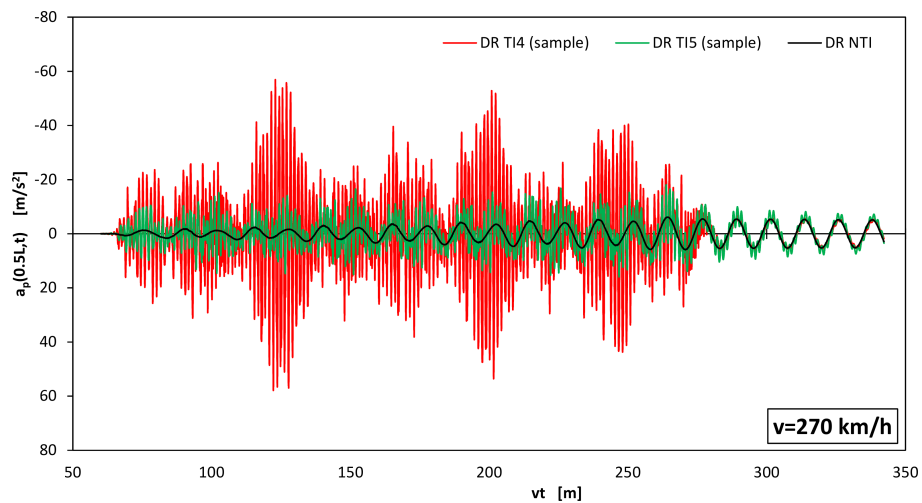


Fig. 13. SCB-15 bridge/ballasted track structure/ICE-3 high-speed train system. Output quantity $a_p(0.5L, t)$ [m/s^2] at resonant service velocity $v_{21} = 270 \text{ km/h}$

M. Podworna and M. Klasztor

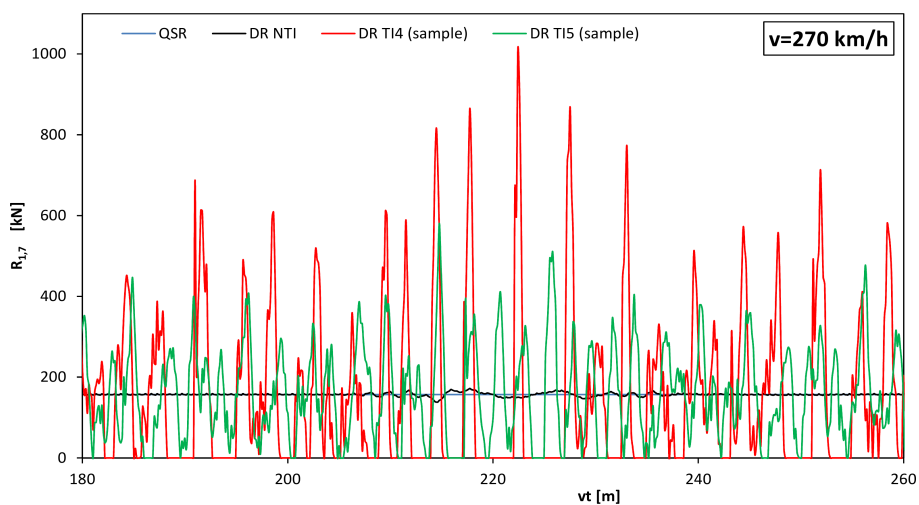


Fig. 14. SCB-15 bridge/ballasted track structure/ICE-3 high-speed train system. Output quantity $R_{1,7}(t)$ [kN] at resonant service velocity $v_{21} = 270$ km/h

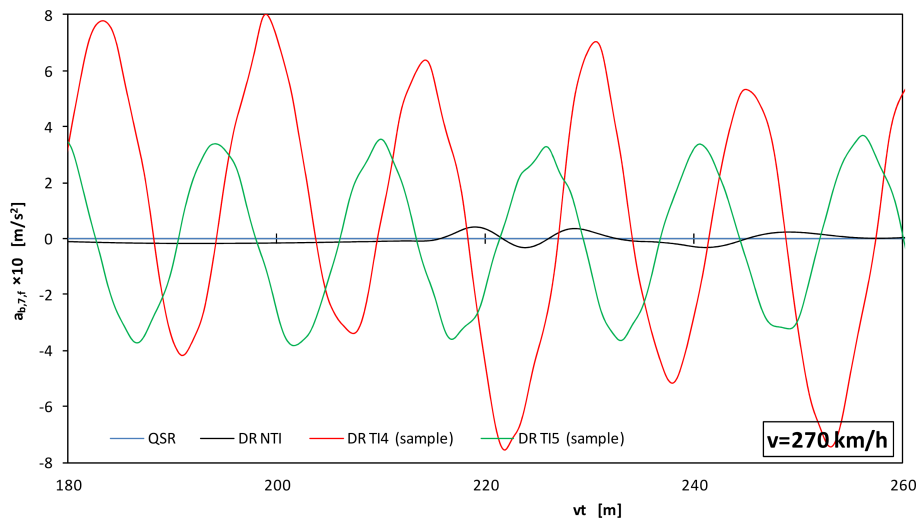


Fig. 15. SCB-15 bridge/ballasted track structure/ICE-3 high-speed train system. Output quantity $a_{b,7,f}(t)$ [m/s^2] at resonant service velocity $v_{21} = 270$ km/h

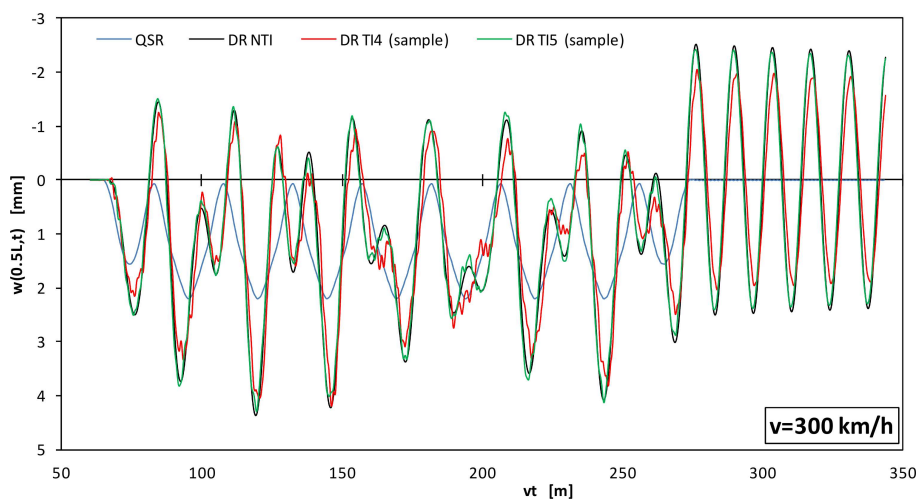


Fig. 16. SCB-15 bridge/ballasted track structure/ICE-3 high-speed train system. Output quantity $w(0.5L,t)$ [mm] at maximum service velocity $v_{\max} = 300$ km/h

Vertical vibrations of composite bridge/track structure/high-speed train systems. Part 3

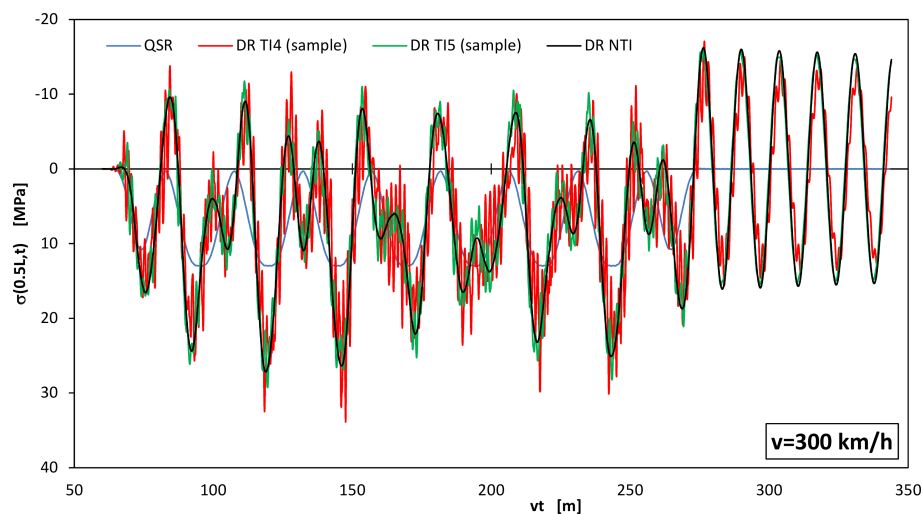


Fig. 17. SCB-15 bridge / ballasted track structure / ICE-3 high-speed train system. Output quantity $\sigma(0.5L, t)$ [MPa] at maximum service velocity $v_{max} = 300$ km/h

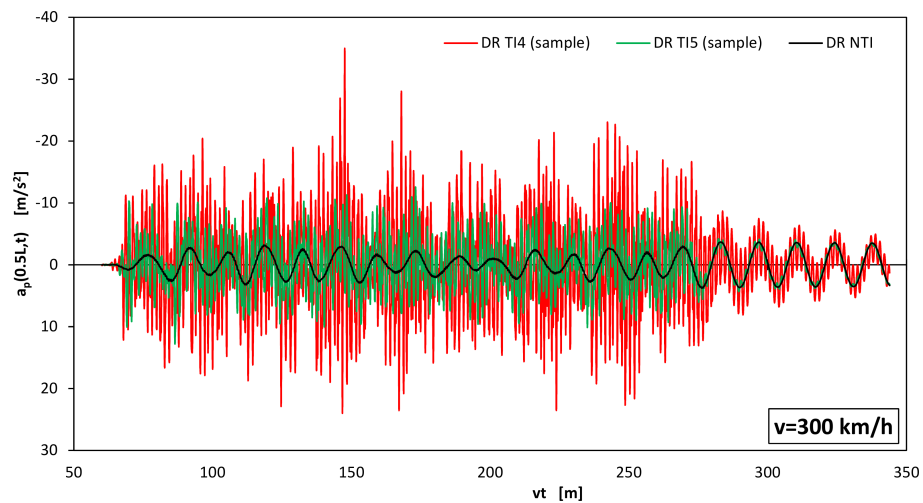


Fig. 18. SCB-15 bridge / ballasted track structure / ICE-3 high-speed train system. Output quantity $a_p(0.5L, t)$ [m/s^2] at maximum service velocity $v_{max} = 300$ km/h

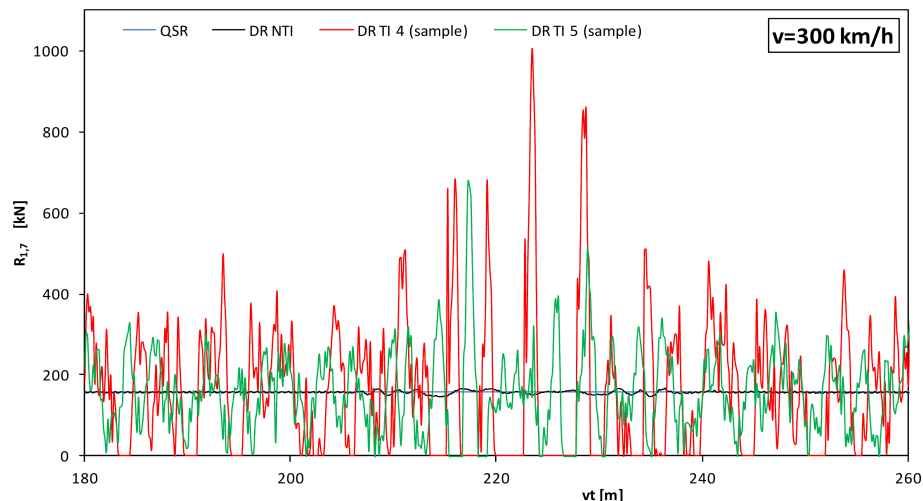


Fig. 19. SCB-15 bridge / ballasted track structure / ICE-3 high-speed train system. Output quantity $R_{1,7}(t)$ [kN] at maximum service velocity $v_{max} = 300$ km/h

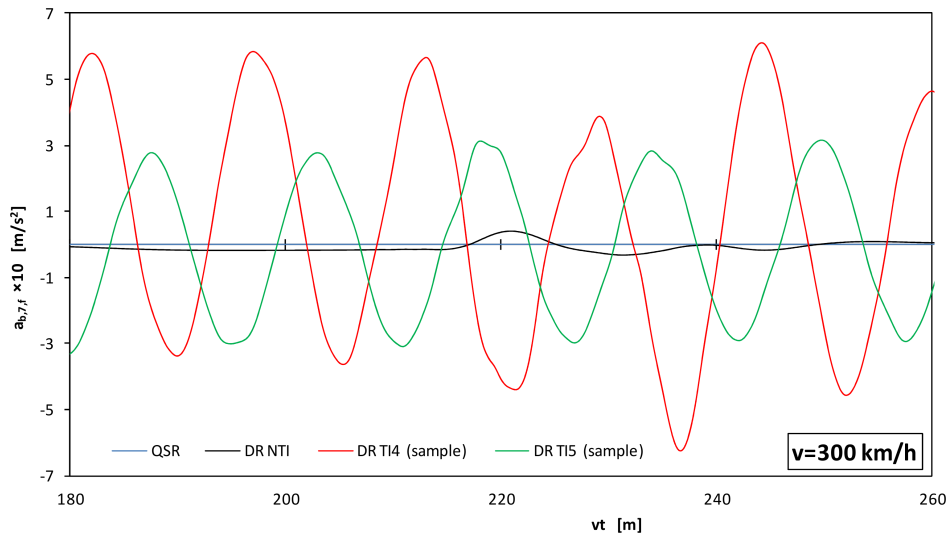


Fig. 20. SCB-15 bridge / ballasted track structure / ICE-3 high-speed train system. Output quantity $a_{b,7,f}(t)$ [m/s^2] at maximum service velocity $v_{max} = 300 \text{ km/h}$

Based on the results presented in Table 7 and in Figs. 6–20 and other results not presented in this study, the following main conclusions are formulated:

1. In the case of a smooth track, the resonant speed 180 km/h is the most disadvantageous in reference to the LCC condition. In the cases of TI6, TI5, or TI4 vertical track irregularities both resonant speeds, 180 and 270 km/h, are disadvantageous in reference to the LCC condition.
2. Random vertical track irregularities mostly cause a slight detuning of the BTT system at resonant operating speeds. At 180 km/h resonant speed, there are high-frequency oscillations of small amplitude in the time-histories of deflections and stresses. In the case of resonance speed of 270 km/h, high-frequency oscillations in the stress time-histories are large.
3. Vertical track irregularities TI6, TI5, or TI4 in the resonant states of the BTT system lead to high-frequency oscillations in the vertical acceleration of the bridge deck. The TSC condition is exceeded more than two times yet in the case of the smooth track, and the deck accelerations grow significantly when vertical track irregularities exist. It may lead to destabilization of the ballast-bed on the bridge.
4. Dynamic pressure forces of the moving wheel sets are quasi-static in the case of an even track (NTI). The TI6 irregularities lead to acceptable decrease of values of these forces in the resonant states. The TI5 irregularities cause high-frequency oscillations in the dynamic pressure force time-histories and series of impacts of the wheel sets onto the rails appear in the response. In the case of TI5, a small number of impacts is observed in resonant states, while the TI4 irregularities induce a large number of impacts. Moreover, the TI4 irregularities result in substantial amplification of the pressure force values. Thus, the instability of motion of wheel sets is possible in the case of TI4 vertical track irregularities at the resonant operating speeds.

5. The PCC condition is fulfilled at very good level for the NTI, TI6, and TI5 cases, and at good level in the TI4 case.

Basic statistics (expectance $E(Z)$, standard deviation $D(Z)$) were estimated of 20 – element sample, for resonant operating velocity $v = 180 \text{ km/h}$ and line grade 4, for the following design quantities: $w_{max}(0.5L)$, $\sigma_{max}(0.5L)$, $a_{p,max}(0.5L)$. The results of the estimation are set up in Table 8. The interval $[Z_l, Z_u]$ includes values of a random variable Z taken from 20 realizations.

Table 8
Estimation of basic statistics of selected design quantities for resonant operating velocity $v = 180 \text{ km/h}$ and line grade 4

Quantity/statistic	TI	$w_{max}(0.5L)$ [mm]	$\sigma_{max}(0.5L)$ [MPa]	$a_{p,max}(0.5L)$ [m/s^2]
Z	NTI	6.74	43.29	7.64
Z_l	TI4	3.02	22.37	11.62
Z_u	TI4	10.79	72.95	27.25
$E(Z)$	TI4	6.94	47.84	19.61
$D(Z)$	TI4	2.12	13.97	3.95
$[Z_u - E(Z)]/D(Z)$	TI4	1.82	1.80	1.93

Based on the results given in Table 8, the following main conclusions can be formulated:

1. Deflections of the SCB-15 bridge do not exceed $L/1380 = 10.87 \text{ mm}$, thus the serviceability condition due to the bridge deflections may be assessed as met for the present resonant and maximum operating speeds.
2. Track irregularities of line grade 4 (TI4) have a big impact on the deflection and the stress in reference to the bridge and a very large impact on the acceleration of the platform.
3. The lower and upper limits of the range $[Z_l, Z_u]$ can be evaluated of the top using the following formulas

$$Z_l = E(Z) - 2D(Z), \quad Z_u = E(Z) + 2D(Z). \quad (20)$$

Verification of the LCC, TSC and PCC conditions for resonant operating velocity $v = 180$ km/h and line grade 4 is presented in Table 9. Symbol Z_{max} denotes admissible value of Z quantity, according to respective condition. The following values are used:

$$\begin{aligned}\sigma_m(0.5L) &= 0.5 \max_t \sigma_s(0.5L, t), \\ \sigma_a(0.5L) &= Z_u - \sigma_m(0.5L),\end{aligned}\quad (21)$$

where Z_u – upper limit calculated with Eq. (20)₂. Equations (21) lead to verification of the LCC condition (13) with a safety margin. In the case of TI4, the impact factors $\varphi_w(0.5L)$, $\varphi_\sigma(0.5L)$ are calculated for respective maximum values Z_u .

Based on the values set up in Table 9, the following main conclusions can be formulated:

1. The resonant operating velocity $v = 180$ km/h induces excessive vibrations of the SCB-15 bridge/ballasted track structure/ICE-3 high-speed train system.
2. In the case of smooth track (NTI), the LCC and PCC conditions are satisfied, while the TSC condition is exceeded twice.
3. In the case of TI4 irregularities the LCC condition is satisfied at the safety coefficient n_s reduced to the value of 1.16. The PCC is satisfied at good level, whereas the TSC condition is exceeded nearly 8 times.

Table 9

Verification of LCC, TSC and PCC conditions for SCB-15 bridge/ballasted track structure/ICE-3 high-speed train system, at resonant operating velocity $v = 180$ km/h and vertical track irregularities of line grade 4

Quantity	Unit	NTI	TI4	Z_{max}	Condition
$\varphi_w(0.5L)$	–	3.06	4.90		
$\varphi_\sigma(0.5L)$	–	3.33	5.61		
$\sigma_m(0.5L)$	MPa	6.50	6.50		
$\sigma_a(0.5L)$	MPa	36.79	69.28		
$\sigma_f(0.5L)$	MPa	126.43	202.78	157	LCC
$a_{p,max}(0.5L)$	m/s^2	7.44	27.51	3.50	TSC
$a_{b,max}$	m/s^2	0.24	1.14	1/1.3/2	PCC

6. General conclusions related to SCB-15 bridge/ballasted track structure/ICE-3 train system

1. The dynamic amplification factor in stress that corresponds to Real Train moving on an even track exceeds value 3 for the resonant operating speed and value 2 for the maximum operating speed.
2. The dynamic amplification factor in stress corresponding to Real Train moving on a track with vertical irregularities TI4 exceeds value 5 for the resonant operating speed and value 2 for the maximum operating speed.
3. The load capacity condition including high-cycle fatigue (durability condition) is satisfied with safety coefficient $n_s = 1.5$ for extraresonant operating speeds and vertical track irregularities of line grades 5 and 6.

4. Random track irregularities generally induce multiple wheel-rail micro-detachment. The wheel-rail pressures have high frequency pulse nature. Wheel-rail separation and impulses do not occur in the case of smooth rails (NTI) and for the smallest track irregularities (TI6).
5. Time-histories of the bridge deck accelerations when vertical track irregularities exist are consistent with well-known experimental results, which adds credibility to the results. Nevertheless, it is pointed out that TSC is weakly satisfied for NTI conditions at high extraresonant operating speeds and exceeded several times at the TI4 conditions.
6. The resonant operating speeds of an ICE-3 train should not be serviced in the cases of lower line grades 5 and 4.
7. The dynamic amplification factor corresponding to the dynamic wheel-rail pressure forces is more than 3 in the case of $v = 180$ km/h and TI4 and more than 5 in the case of $v = 300$ km/h and TI4. Thus, track irregularities of line grade 4 should not be permitted for the resonant and high operating speeds. In these conditions, accelerated degradation of the rail and wheel rolling surfaces is predicted.
8. A problem of possible destabilization of macadam ballast-beds on railway bridges needs to find any structural solution. One of possible solution is applying the German RHEDA-2000 ballastless track structure.
9. Dynamic phenomena in the bridge/ballasted track structure/high-speed train system require experimental investigations focussed on identification/validation/verification problems. Such investigations are difficult, time-consuming and expensive and can be performed by an international research team.

Acknowledgements. The study was supported by the National Centre for Science, Poland, as a part of the project No. N N506 0992 40, realized within the period 2011–2013. This support is gratefully acknowledged.

REFERENCES

- [1] F.T.K. Au, J.J. Wang, and Y.K. Cheung, “Impact study of cable stayed railway bridges with random rail irregularities”, *Engineering Structures* 24, 529–541 (2002).
- [2] C. Esveld, “Measuring and rectifying rail roughness and bad welds”, *Proc. 3rd Int. Heavy Haul Railways Conf.*, Paper BIB-52, CD-ROM (1986).
- [3] L. Fryba, *Dynamics of Railway Bridges*, Academia, Praha, 1996.
- [4] M. Klasztorny, *Dynamics of Beam Bridges Loaded by High-Speed Trains*, WNT Press, Warsaw, 2005, (in Polish).
- [5] X. Lei and N.-A. Noda, “Analyses of dynamic response of vehicle and track coupling system with random irregularity of track vertical profile”, *J. Sound Vib.* 258 (1), 147–165 (2002).
- [6] F. Lu, J.H. Lin, D. Kennedy, and F.W. Williams, “An algorithm to study non-stationary random vibrations of vehicle – bridge system”, *Comput. Struct.* 87, 177–185 (2009).
- [7] A. Matsuuura, “Dynamic behaviour of bridge girder for high speed railway bridge”, *RTRI Quarterly Reports* 20 (1), 70–76 (1979).
- [8] M. Podworna and M. Klasztorny, “Vertical vibrations of composite bridge/track structure/high-speed train system. Part 1:

- Series-of-types of steel-concrete bridges”, *Bull. Pol. Ac.: Tech.* 62 (1), 165–180 (2014).
- [9] M. Podworna and M. Klasztorny, “Vertical vibrations of composite bridge/track structure/high-speed train system. Part 2: Physical and mathematical modelling”, *Bull. Pol. Ac.: Tech.* 62 (1), 181–196 (2014).
- [10] M. Podworna and M. Klasztorny, and D. Bryja, “Modelling of composite bridges loaded by high-speed trains including random track irregularities”, *Research Report No SPR/8/2013*, Institute of Civil Engineering, Wroclaw University of Technology, Wroclaw, 2013, (in Polish).
- [11] M.-K. Song, H.-C. Noh, and C.-K. Choi, “A new three dimensional finite element analysis model of high-speed train – bridge interactions”, *Engineering Structures* 25, 1611–1626 (2003).
- [12] A. Wiriyachai, K.H. Chu, and V.K. Gang, “Bridge impact due to wheel and track irregularities”, *ASCE J. Engng. Mech. Div.* 108 (4), 648–666 (1982).
- [13] Q.-L. Zhang, A. Vrouwenvelder, and J. Wardenier, “Numerical simulation of train – bridge interactive dynamics”, *Comput. Struct.* 79, 1059–1075 (2001).
- [14] Y.-W. Zhang, J.-H. Lin, Y. Zhao, D.P. Howson, and F.W. Williams, “Symplectic random vibration analysis of a vehicle moving on an infinitely long periodic track”, *J. Sound Vib.* 329, 4440–4454 (2010).